Journal of Luminescence 203 (2018) 135–144

Contents lists available at ScienceDirect

Journal of Luminescence

journal homepage: www.elsevier.com/locate/jlumin

A review on pedestal waveguides for low loss optical guiding, optical amplifiers and nonlinear optics applications

Daniel O. Carvalho[a], Luciana R.P. Kassab[b,*], Vanessa D. Del Cacho[b], Davinson M. da Silva[b], Marco I. Alayo[c]

[a] Univ. Estadual Paulista Júlio de Mesquita Filho (UNESP), Sao Joao da Boa Vista, SP 13876-750, Brazil
[b] Faculdade de Tecnologia de São Paulo, CEETEPS/UNESP, 01124-060 São Paulo, Brazil
[c] Escola Politécnica, Universidade de São Paulo (USP), 05508-010 São Paulo, Brazil

ARTICLE INFO

Keywords:
Pedestal waveguides
Rare earth ions luminescence enhancement
Optical amplifiers
Gain enhancement due to gold nanoparticles
Integrated nonlinear optics

ABSTRACT

In this work we review the recent advances and demonstrate possible future perspectives regarding pedestal waveguide fabrication technology. The optical waveguides produced using this technology represent a new platform to study novel optical materials that could not be explored differently as this fabrication process does not require etching of the core material itself. Thus, novel materials that are highly inert to chemical etchants, such as those composed of heavy metal elements, can be used with this new architecture that allows the fabrication of integrated optical devices. Lower propagation losses with pedestal waveguides when compared to rib waveguides are reviewed. The possibility to construct Mach-Zehnder interferometer structures using the pedestal waveguide technology is shown. The optical amplifiers with high gain are demonstrated using this pedestal process. Furthermore, using the pedestal architecture, it is presented the possibility to produce rare earth ions doped waveguides with gold nanoparticles, which demonstrated gain enhancement attributed to the efficient luminescence due to gold nanoparticles, thus opening possibilities for potential applications in integrated photonics. Finally, another research field that could benefit greatly in the near future from this new architecture is the integrated nonlinear optics as the pedestal waveguide fabrication technology opens up the possibility of using novel materials with high optical nonlinear susceptibilities.

1. Introduction

Recently the optical community has shown a very high demand for novel material platforms for the development of different areas of photonics. This is especially true for the fields of optical amplification and nonlinear optics. Doped fiber amplifiers such as Erbium Doped Fiber Amplifiers (EDFAs) and Ytterbium Doped Fiber Amplifiers (YDFAs) have become key components of optical communication networks. A natural step is to integrate these devices in photonic chips for miniaturization and to compensate for optical losses in integrated photonic devices. New host materials based on heavy metals are of much interest in this area [1] since they may present high nonlinear optical susceptibilities, which is important for applications like parametric amplification, wavelength conversion, all-optical switching, among others [2–7]. Heavy metal oxide glasses [8,9] exhibit adequate thermal properties, mechanical strength and chemical durability, can be melted in ambient atmosphere requiring no sophisticated apparatus, present low phonon energy and high refractive index, and are suitable hosts for rare-earth ions. Consequently, several studies on heavy metal oxide glasses [10–14] and also on heavy metal oxyfluoride glasses [15,16] were conducted motivated by the desire to identify low phonon energy hosts that have large mechanical strength, low manufacturing temperatures and high refractive index. Recently, considerable emphasis has been given to the discovery of new heavy metal oxide glass compositions to be used as rare-earth ions doped luminescent hosts. Important features that make them suitable for devices fabrication and attracted several researches are their relatively high refractive index ($\geq$ 1.8), high dispersion, low melting temperatures (normally in the range 700–1200 °C), wide transmission window (visible to mid - infrared), and low cutoff phonon energy (500–800 cm^{-1}) among oxide glass formers. The reduced phonon energy increases the efficiency of luminescence and provides the possibility to develop more efficient visible optical lasers; normally frequency upconversion photoluminescence is more efficient in these hosts. Heavy metal oxide glasses are also suitable for white light generation and can replace the conventional incandescent and fluorescent lamps [17,18]. Particularly because of their

* Corresponding author.
E-mail address: kassablm@osite.com.br (L.R.P. Kassab).

https://doi.org/10.1016/j.jlumin.2018.06.037
Received 1 April 2018; Received in revised form 14 June 2018; Accepted 14 June 2018
Available online 18 June 2018

potential for laser hosts, tellurite and germanate glasses have been the subject of several investigations [19–22].

On the other hand, it is well known that materials prepared with metallic elements are prone to problems during the etching process used to define the waveguide sidewalls. This is essentially due to micro-masking caused by atoms of metallic elements which lead to: rough etched surfaces and defects, commonly known as “grass”, (because of its resemblance to actual grass), formed on the top of the etched regions [23]. This artifact is detrimental to light propagation inside the waveguides, as they lead to scattering and radiation losses. Properly designed pedestal waveguides have been shown to mitigate significantly these effects [24]. Other configurations used to fabricate waveguides have been proposed in which hollow core arrows are fabricated over self-aligned pedestals (SAP) [25], resulting in a minimization of the waveguides propagation losses. Nonetheless, as stated, this concept has not been applied to solid core waveguides and this process is slightly different from the pedestal process.

With the pedestal waveguide fabrication technology, the definition of the waveguide sidewalls is performed on the lower cladding by the construction of a pedestal using conventional photolithography and Reactive Ion Etching (RIE) techniques. The core is deposited after the definition of the pedestal, no longer being necessary the etching of this layer and thus resulting in rounded sidewalls. Since the light propagating in the core does not interact with etched sidewalls, lower propagation losses can be achieved when compared to conventional rib or strip waveguides fabricated with similar processing steps.

Furthermore, devices with applications on integrated nonlinear optics have attracted much attention over the last decade. By allowing a larger refractive index contrast between core and cladding materials, when compared to the typical optical fibers, integrated devices tend to have far smaller transverse mode dimensions. Consequently, larger nonlinear parameters can be achieved, which means that shorter devices could be used with similar efficiencies. Silicon On Insulator (SOI) was the first material platform used for integrated nonlinear optics. Devices for wide-band optical amplification, wavelength conversion as well as multiple wavelength coherent optical sources have been demonstrated using this platform [26–28]. Although silicon, which is used as the core material in SOI devices, has a very large nonlinear response, it suffers from high nonlinear losses and does not operate over a large bandwidth due to its narrow band-gap.

Also, other platforms have been explored for nonlinear optical applications. Among the materials that are potential candidates for nonlinear optical applications, Silicon Nitride (Si_3N_4) and Hydex deserve attention. However, both have advantages and disadvantages [29,30]. These platforms have been used in the fabrication of devices to demonstrate parametric amplification, wavelength conversion and Frequency Comb Generation and have shown a much wider band of operation than silicon [31–33]. Furthermore, since these platforms use silicon nitride and oxynitride materials, they are easily etched using conventional Reactive Ion Etching (RIE) technique with fluorinated gases, leading to very low loss waveguides. On the other hand, one could say that there is still a lot to be done on integrated nonlinear photonics, and if other materials are to be explored, novel techniques for fabricating waveguides will have to be used.

The pedestal process has potential to be hugely beneficial for materials that have been proposed as high-k dielectrics for MOS transistors and capacitors because of their high optical nonlinear susceptibilities.

Finally, besides holding great promise for the exploration of novel material platforms for optical amplifier and nonlinear optical devices, the pedestal process can be used to diminish the propagation losses of photonic waveguides. In fact, this was the original reason for proposing this fabrication technique. Waveguides with losses as low as half of those obtained for rib waveguides fabricated under the same conditions have been demonstrated this way [32]. Mach-Zehnder interferometer structures using $TeO_2-WO_3-Bi_2O_3$ core fabricated with pedestal waveguide technology, exhibited low propagation losses at 633 and 1050 nm and demonstrated possible applications as integrated optical sensors [34]. Also, fabrication of Yb^{3+}/Er^{3+} codoped $TeO_2-WO_3-Bi_2O_3$ pedestal waveguides showed applications as optical amplifiers at 1530 nm [35] and advances on the fabrication process of Yb^{3+}/Er^{3+} codoped GeO_2-PbO pedestal waveguides reported the possibility to enhance the gain at about 50%, at 1530 nm [1]. Finally, the influence of gold nanoparticles on Yb^{3+}/Tm^{3+} codoped GeO_2-PbO pedestal waveguides was reported more recently. In this case the high luminescence and gain enhancement, at 805 nm, due to the presence of gold nanoparticles showed relevant results for the development of optical amplifiers to be used in integrated optics, especially on optical network at short distances [36].

We remark that Begou et. al. [37] performed a theoretical study of pedestal waveguides. In this study an extension of Marcatili's [38] method was developed in order to adapt it to pedestal structures. Simulations were performed for two different T-pedestal waveguide (T-PW) configurations corresponding respectively to a high and a lower core to pedestal widths ratio. Then the extended Marcatili method was compared with a semi-vectorial finite difference method (SVFD) [39] and a spectral method developed by Galerkin [40–42]. By using all this approach the authors found a good agreement between Marcatili's method and the numerical methods. Finally these three approaches were used to study the modal birefringence minimization for pedestal structures. The study showed that when the core height or core width, are high enough the pedestal does not play a significant role on the modal birefringence.

2. Pedestal waveguides fabrication process

The first step of the pedestal waveguides fabrication process using silicon technology is the thermal growth on a silicon substrate of a relatively thick silicon dioxide film (1–2 μm-thick) with refractive index of 1.46 [1,24,34–36]. It is worth mentioning that there is no restriction with respect to the use of other material platforms than silicon since the same concept can be applied to other materials. However, when silicon technology is used, thermal oxidation is normally preferred over Plasma Enhanced Chemical Vapor Deposition (PECVD) or Low Pressure Chemical Vapor Deposition (LPCVD) techniques to grow silicon dioxide because it leads to films with the smallest absorption losses.

The pedestals are defined by RIE technique on the lower cladding layer. In the previous studies that are reviewed in this work, this step has been done using chromium as hard-mask, due to its high selectivity in the oxide etching. The chromium film can be deposited by RF magnetron sputtering or evaporated. After this, the sidewalls of the pedestal are defined using optical contact lithography. A few issues arise due to the use of chromium hard-mask, despite its good selectivity. One of these issues is related to the effect of the oxide micro-masking surrounding the waveguide [23]. Basically, chromium particles sputtered off from the hard-mask are deposited over the surrounding region and act locally as micro-masks. So, after the etching process, pillar shaped structures in the form of “grass” can appear in the film being etched. Another related issue is that using metal hard-mask results in larger values of sidewall roughness than using resist masks [43].

Both these issues could be overcome by the choice of a better masking material such as a resist with better selectivity, which would certainly result in lower propagation losses. The RIE etching of the lower cladding to form the pedestal on the top of the silicon dioxide substrate is illustrated in Fig. 1a. This step is followed by the removal of the chromium mask. The silica layer can be partially or completely etched. In some cases, etching the silica layer and some of the silicon substrate can lead to lower propagation losses [32]. After defining the pedestal, the succeeding step is the core layer deposition, as illustrated in Fig. 1b. In this Figure some portions of the film that composes the core of the pedestal waveguide were removed in order to make the shape of the waveguide cross-section evident. The ring resonator shape

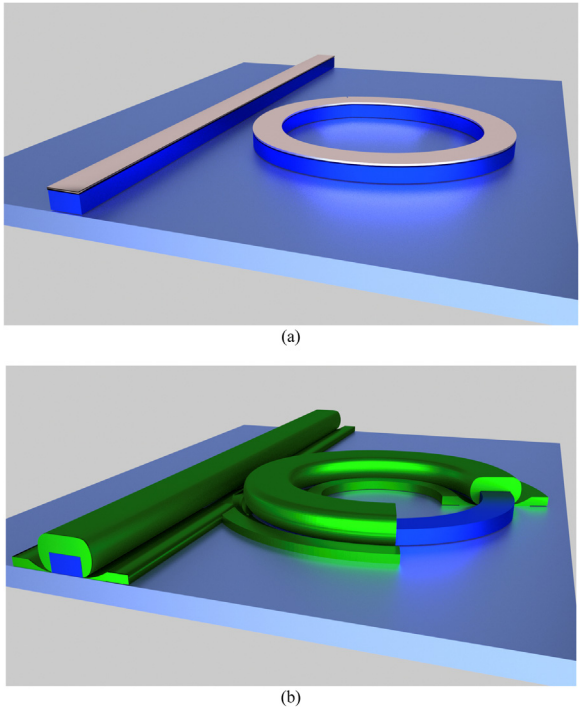

Fig. 1. Pedestal waveguide fabrication process. (a) Etching of the lower cladding to form the pedestal. (b) Deposition of the core material. Some portions of the film that composes the core were removed for clarity.

is used only as illustration of an actual device in this case. It is important to notice that in order to fabricate ring resonators using pedestal waveguide it will be essential to develop a way to accurately define the gap between the ring structure and the bus waveguide, due to the fact that the core is deposited after the definition of the pedestal, and thus, an increase in the core thickness will translate into a reduction of the aforementioned gap.

Different materials such as silicon oxide, aluminum nitride, tellurite and germanate glasses have been used as core in previous works [1,24,34–36,44,45]. Since the material does not need to be etched in the pedestal waveguide fabrication, many different materials could be used as core, as long as the refractive index is higher than that of the pedestal. On the other hand, it is possible to use materials that have the same refractive index as that of the pedestal if an arrow type structure is used for light confinement [45]. To make the losses even smaller and protect the waveguide core, which is required in most applications, an upper cladding layer can be deposited on top of the core.

It is noteworthy that the fabrication process of pedestal waveguides encompasses the same number of steps as those of a regular etched core integrated Photonic waveguide. In fact, the fabrication procedures are the same except for the fact that they are done in a different order: the deposition of the core layer is performed after the etching for the definition of the sidewalls.

The first solid core pedestal ever fabricated was a solid core arrow waveguide type pedestal (Fig. 2) [24]. In this type of waveguide, the refractive index of the core is the same as that of the pedestal and an anti-resonant layer is deposited on the top of the pedestal before the deposition of the core. This waveguide has the advantage of the virtual single-mode operation whereby all the higher order modes are suppressed due to their low reflectivity with respect to the anti-resonant layers. In fact, light pertaining to these modes leak towards the substrate. The core of these waveguides was composed of silica and propagation losses as low as 0.45 dB cm^{-1} were obtained at the wavelength of 633 nm. Three different pedestal heights were tested (3, 4 and 5 μm) and the smallest losses were obtained with the smallest height. The losses obtained are half of those of regular arrow [46] waveguides

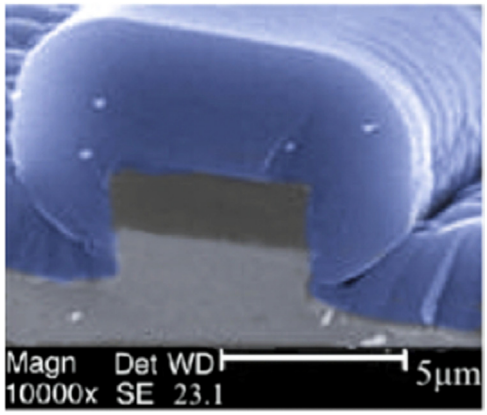

Fig. 2. Arrow pedestal waveguide fabricated with silicon dioxide core (taken from [24]).

essentially due to the fact that the mode was surrounded by deposited sidewalls rather than etched ones. Optical waveguides with varying widths were tested and single mode operation was observed for pedestal widths equal to or smaller than 6 μm. From the measured and simulated mode profile it is possible to see that the interaction of the mode with the etched sidewalls of the pedestal is almost negligible.

Another important aspect to point out is that the pedestal waveguide that we have been fabricating is very different from other waveguides produced over self-sustained pedestals reported in the literature. In [47] for example, “pedestal-supported waveguides” have been proposed for single polarization transmission. These waveguides are silicon-core waveguides fabricated using the same procedure used for etched-core strip waveguides with an additional step of wet etching for the silica film underneath. This type of waveguide has interesting polarization properties, but the core is etched just as in a regular waveguide. For this reason, it does not present the same properties in terms of smooth deposited sidewalls as the pedestal waveguides that we have been reporting. In a different work [48], waveguides with a core etched all the way with part of the lower cladding were proposed and were found to have low birefringence. However these different pedestal waveguides do not allow the use of materials that are inert to etchant chemistries or are difficult to etch. We thus consider that the main attractive feature of the pedestal waveguide proposed by us, as demonstrated in recent reports [1,24,34–36,49,50], is the possibility to use any optical material as core layer, even those that are difficult to be etched.

Finally, we remark that light guiding in pedestal based optical structures is due to the Total Internal Reflection (TIR) principle, just as other optical waveguides structures [51] in which light guiding occurs because of the high difference of refractive index values between the core layer (~ 2.0), the lower-cladding layer, formed by the pedestal structure (~ 1.46) and the upper-cladding layer over the core layer which can be the air (1.0) or any other layer with refractive index lower than the core layer. This difference between the refractive indexes allows light guiding in the core layer and prevents the leakage into the pedestal structure. So, as this contrast between the refractive indexes plays a relevant role on the waveguide performance, it is important to choose core materials with refractive index higher than those of the cladding layers. Moreover, the pedestal height and the core layer thickness can have considerable effects on the propagation loss, internal gain and on the number of the optical waveguides modes, such as it was already shown in previous works [1,45]. In this paper we review results of pedestal waveguides whose cores have refractive index around 2.0, and that were fabricated using heavy metal oxide elements on their compositions (GeO_2-PbO and Bi_2O_3-WO_3-TeO_2).

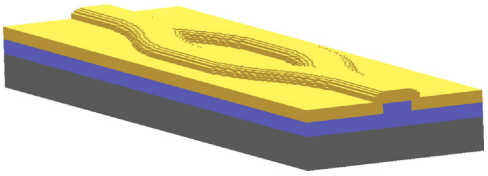

Fig. 3. Schematic diagram of Mach Zehnder structures fabricated using TWB pedestal waveguides (606 nm-core height and 1.05 μm-pedestal height) [34].

3. Using the pedestal technique on the fabrication of integrated optical devices and a comparison with other techniques

Recently, rare earth ion doped amplifiers with two different host materials and dopants have been demonstrated using pedestal waveguides fabrication procedure described above: tellurite based glasses ($TeO_2-WO_3-Bi_2O_3$) [34,35] and germanate based glasses ($PbO-GeO_2$) [1,36,49,50]. Different dopants have been used as well: Thulium (Tm^{3+}), Ytterbium (Yb^{3+}) and Erbium (Er^{3+}). As far as we are concerned the reports of rare earth ions doped pedestal waveguides with and without gold nanoparticles are the ones that are reviewed in the present work section.

These glasses have interesting characteristics, which make them good candidates as hosts for doped amplifiers. Their relatively high refractive index ($n > 2.0$) make them appropriate for allowing highly confined optical modes. They also have a small phonon energy (600–900 cm^{-1}), are chemically inert, and have a high optical transmittance in a wide region of the spectrum, which allow their use for wavelengths extending into the mid-infrared (400–6000 nm).

Mach Zehnder structures (Fig. 3) were fabricated using $TeO_2-WO_3-Bi_2O_3$ pedestal waveguides [34] with different pedestal widths. The purpose of this study was to ensure that low loss pedestal waveguides could be made with tellurite based materials, for applications as integrated optical sensors. Propagation losses were determined using the top view technique [52] and the experimental setup is presented in Fig. 4. The same setup was used for the modal analysis and, in this case, the CCD was positioned in front of the objective lens. Losses as low as 2.0 dB cm^{-1} and 2.5 dB cm^{-1} were obtained at visible (633 nm) and near-infrared (1.05 μm) wavelengths, respectively. Single-mode behavior was observed for waveguide widths up to 5 μm. Fig. 5 presents images obtained from scanning electron microscope (SEM) of the TeO_2-WO_3-Bi_2O_3 pedestal waveguides (606 nm-core height and 1.05 μm-pedestal height) [34].

Note that, opposed to the first pedestals fabricated in [24], where Plasma Enhanced Chemical Vapor Deposition (PECVD) technique was used for the deposition of the silica film used as waveguide core, in the aforementioned studies [1,34–36], the core was deposited using the sputtering technique. This demonstrates that the concept of pedestal can be used with different deposition techniques. As can be seen by comparing Figs. 2 and 5, both the core thickness and the deposition technique influence the geometric shape of the core layer deposited above the pedestal. The width and the height of the pedestal have also a significant effect in the shape of the core layer.

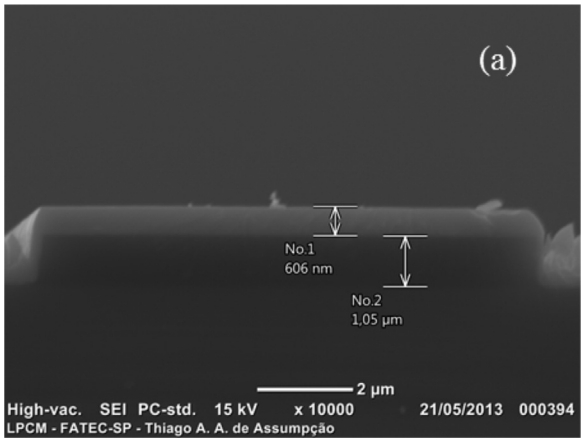

Fig. 5. SEM image of the TWB pedestal waveguide structures (606 nm-core height and 1.05 μm-pedestal height) [34].

Yb^{3+}/Er^{3+} codoped $TeO_2-WO_3-Bi_2O_3$ pedestal waveguides fabricated for optical amplifier applications at 1530 nm were also reported [35]. Losses as low as 2.0 dB cm^{-1} and 2.5 dB cm^{-1} were obtained at visible (633 nm) and near-infrared (1.05 μm) wavelengths, respectively, for waveguide widths within the range of 20–100 μm. For pedestal widths up to 10 μm and 12 μm, single mode waveguides could be obtained at 633 nm and 1050 nm, respectively. Larger waveguide widths provided multimode propagation. The luminescence spectrum due to the $^4I_{13/2} \rightarrow {}^4I_{15/2}$ transition of Er^{3+} ions, centered at 1.53 μm was measured and corroborated the incorporation of rare-earth ions in trivalent form (Fig. 6). Gain of 3.7 dB cm^{-1} was achieved at 1530 nm, under 980 nm excitation, for waveguides width of 20 μm, core height of 0.58 μm and Er^{3+} concentration of 5.0×10^{18} ions.cm^{-3} (Fig. 7). Results of TeO_2 rib waveguides exhibited lower gain (3.0 dB cm^{-1}) [53], even using pump power two orders of magnitude higher (200 mW) and Er^{3+} concentration of $2.2 \times 10^{2\circ}$ ions.cm^{-3}, which is more than four times higher than the previous studies with the same material. It is likely that the use of the pedestal geometry combined with the presence of the Yb^{3+} sensitizer (4.2×10^{20} ions.cm^{-3}) might have contributed to

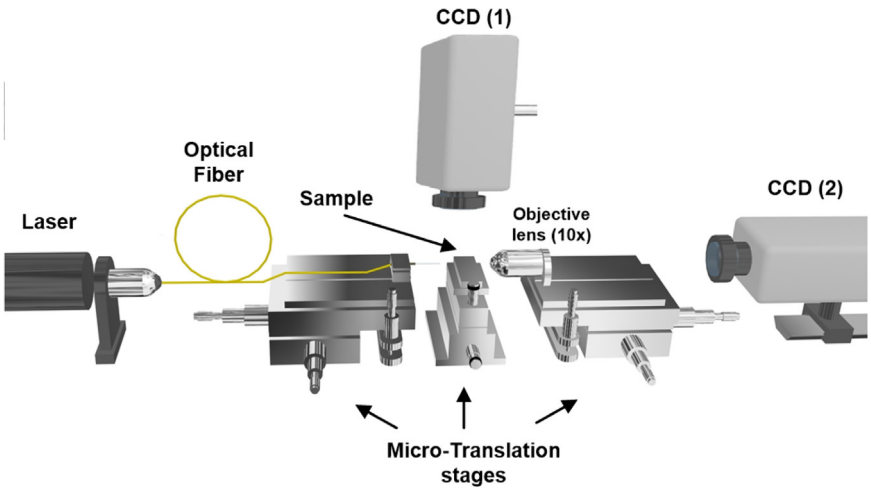

Fig. 4. Experimental setup used for the propagation loss measurements and also for the modal analysis using the top view technique [34].

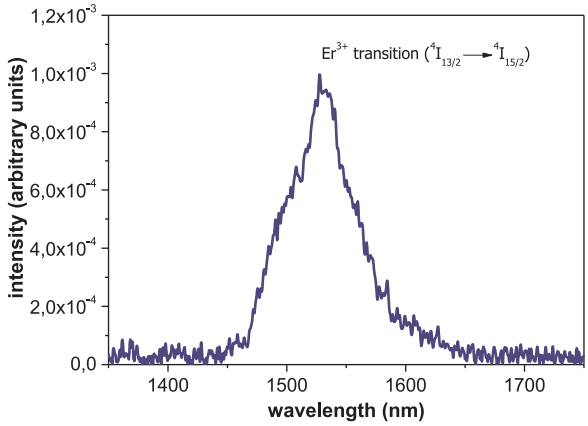

Fig. 6. Luminescence spectrum of Yb^{3+}/Er^{3+} codoped Bi_2O_3-WO_3-TeO_2 pedestal waveguide at 1530 nm [35].

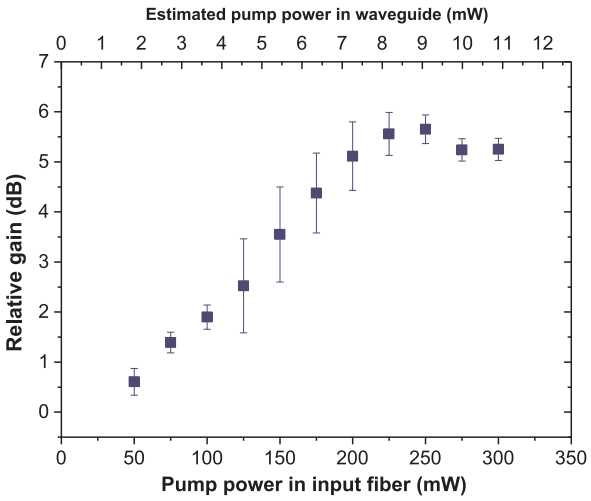

Fig. 7. Relative gain of Yb^{3+}/Er^{3+} codoped Bi_2O_3-WO_3-TeO_2 pedestal waveguides under 980 nm excitation (18 μm waveguide width) [35].

the gain enhancement [35].

The PbO-GeO_2 host is the other material that has been used for rare earth ions incorporation in order to fabricate pedestal waveguide-based amplifiers. Germanate glasses also have high refractive index (n = 2.0) which enables high confined optical modes. Low cut phonon energy (800 –900 cm^{-1}), high chemical stability and mechanical durability are also some characteristics that make them attracting materials for photonics applications. Like tellurite materials they can be used for wavelengths extending into the mid-infrared applications because of the low absorption within the range of 400–5000 nm [1,36,49,50]

Optical amplifiers based on $PbO-GeO_2$ pedestal waveguides codoped with Er^{3+}/Yb^{3+} were fabricated. In this case advances on the fabrication process were performed [1]. To show this, it was reported a comparison between two different groups of $PbO-GeO_2$ pedestal waveguides codoped with Er^{3+}/Yb^{3+}, entitled GP-A and GP-B, that were fabricated under different process parameters [1]. In both cases the pedestal structure was defined by CHF_3/O_2 plasma etching using RIE technique. For the etching of the silicon oxide of the GP-A sample, it was used an RF power of 100 W and gas flow rate of 40 sccm for both CHF_3 and O_2, under a chamber pressure of 50 mTorr using 2 steps of 30 min for GP-A and 3 steps of 30 min for GP-B. SEM images of the waveguides are shown in Fig. 8. The core surface presented low roughness in both cases. However, pillar structures adjacent to the lateral surface of GP-A waveguide were observed (Fig. 8a) and were attributed to micromasking effects [23] (columnar growth due to the incomplete removal of chromium mask layer). The presence of these

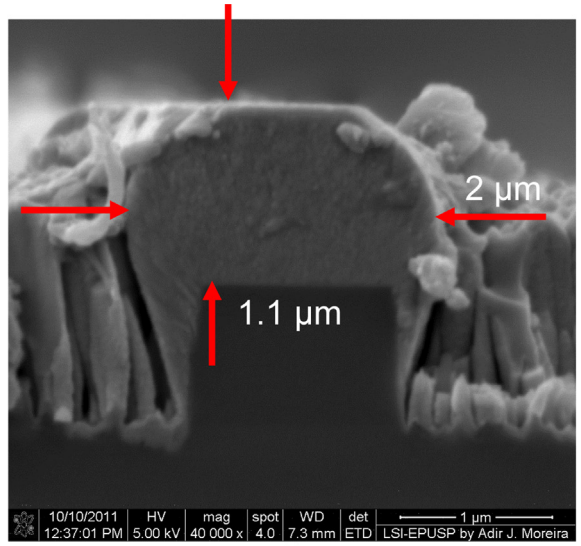

(a)

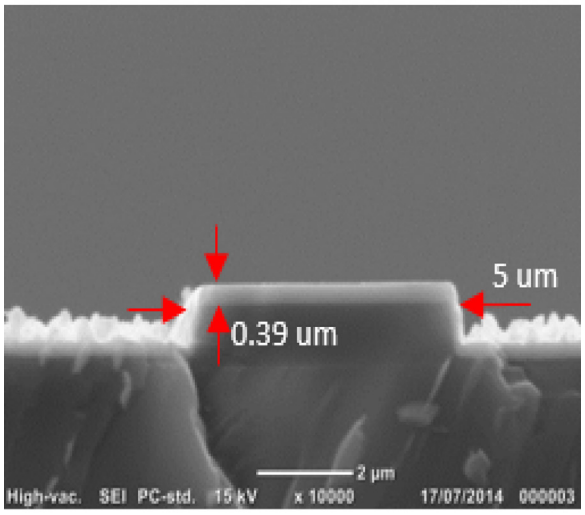

(b)

Fig. 8. SEM images of (a) GP-A and (b) GP-B pedestal waveguides (values of core width and core height are shown) [1].

structures can compromise the guiding as their proximity to the optical field confined in the core layer may enhance propagation losses, due to radiation leakage [54]. The thickness of chromium mask layer was reduced by 70% in comparison to the one used in GP-A, in order to decrease this effect. Also, the pedestal height was increased to 1.1 μm in GP-B (for GP-A waveguide this value was 0.9 μm). At last, the thickness of the core layer was reduced in GP-B to 0.39 μm (for GP-A this value is 1.1 μm). Fig. 8b shows that pillar structures were also present in GP-B waveguide. However, they are isolated from the guided light in the core layer, differently from GP-A waveguide. Propagation losses at 632 and 1068 nm are shown in Fig. 9. Fig. 10 shows the results of the gain at 1530 nm (980 nm excitation), as a function of the pump power in the 70 μm-wide pedestal waveguides. Gain of 4.0 dB/cm and 6.0 dB/cm were obtained for waveguide width of 70 μm, for GP-A and GP-B, respectively. That report showed that the improvement of the fabrication process contributed to enhance the performance of the pedestal waveguides, as a reduction of about 50% was observed for the propagation losses at 632 and 1068 nm, whereas enhancement of approximately 50% was obtained for the gain at 1530 nm [1].

Using the same optimized procedure for the fabrication of the pedestal waveguide, PbO-GeO_2 waveguides codoped with Ym^{3+}/Tm^{3+}

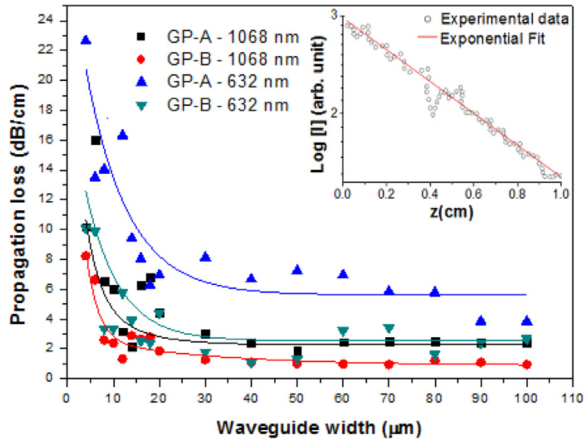

Fig. 9. Propagation loss results of GP-A and GP- B pedestal waveguides in the 4–100 μm width range; the inset shows the slope of the measured light intensity, captured by the CCD camera, as a function of the waveguide length (z) [1].

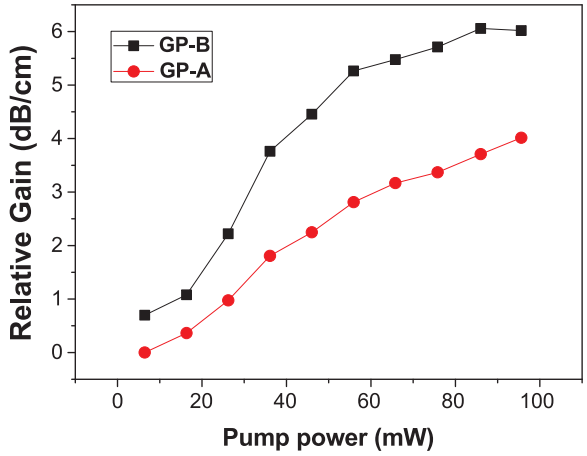

Fig. 10. Relative gain for 70 μm waveguide width GP-A and GP-B pedestal waveguides [1].

with and without gold nanoparticles were produced [36]. The nucleation of gold nanoparticles was performed with adequate annealing after the melting quenching procedure. This annealing normally made in the vicinity of the glass transition temperature demonstrated to be efficient and was successfully used in germanate and tellurite glasses [55–58]. The same method of nucleation was applied for thin films produced by RF sputtering [59–61].

In order to cover the core of PbO-GeO_2 waveguides codoped with Ym^{3+}/Tm^{3+} with a gold thin film, it was used the sputtering technique with 5 W applied to a commercial high purity gold target during 10 and 20 min. After this procedure the waveguide was heat treated for 1 h to reduce the Au^{+} or Au^{3+} ions to Au^{0} and to nucleate gold nanoparticles. Fig. 11 shows the luminescence enhancement of Tm^{3+} ions transitions centered at 470 nm ($^1G_4 \rightarrow {}^3H_6$), 647 nm ($^1G_4 \rightarrow {}^3F_4$) and 793 nm ($^3H_4 \rightarrow {}^3H_6$) due to the presence of gold nanoparticles because of the local field growth in the vicinities of the nanoparticles. It was noted enhancement factor of around 129%, for the emission band centered at ≈ 470 nm, of 225% for the emission band centered at 647 nm and of 21% for the one at 793 nm. The highest enhancement observed for the emission bands at 470 and 647 nm was attributed to the highest proximity with the localized surface plasmon resonance of gold nanoparticles (~ 500 nm) [19]. In this case no energy transfer between gold nanoparticles and the rare earth ions was expected, because of the large difference between the excitation wavelength (980 nm) and the one of the localized surface plasmon. Relative gain enhancement of more than

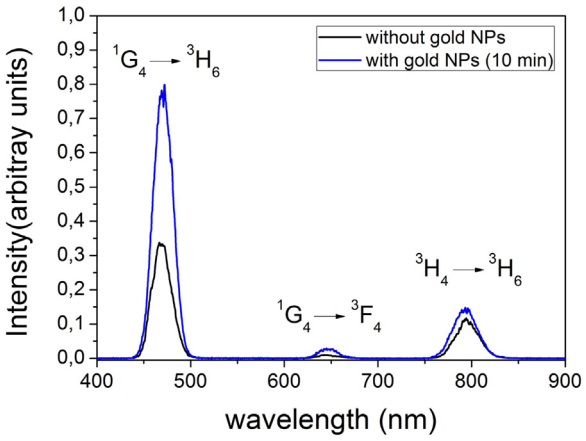

Fig. 11. The luminescence of Tm^{3+}/Yb^{3+} doped PbO-GeO_2 thin films, with and without gold nanoparticles, under 980 nm excitation.

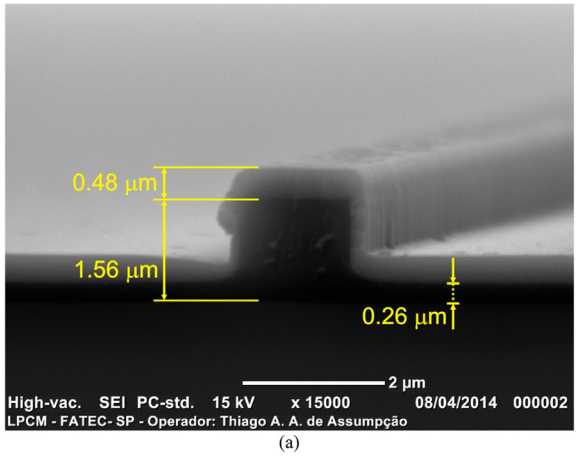

(a)

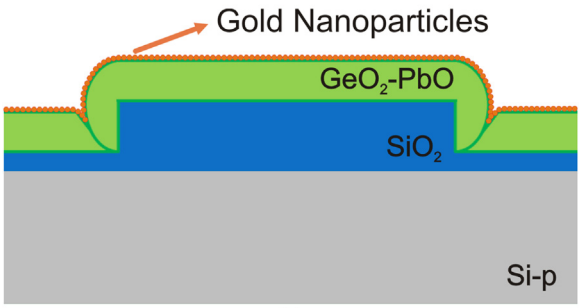

(b)

Fig. 12. (a) SEM image showing the profile of PbO-GeO_2 waveguide; (b) Front–view illustration of Tm^{3+}/Yb^{3+} codoped PbO-GeO_2 pedestal waveguides with gold nanoparticles [36].

100% was observed due to the presence of gold nanoparticles. Fig. 12(a) shows the results of scanning electron microscopy (SEM) measurements (0.48 μm height for the core and 1.56 μm for the SiO_2 thermally grown layer). Fig. 12(b) shows the front-view illustration of Tm^{3+}/Yb^{3+} codoped PbO-GeO_2 waveguide with the thin gold film. The propagation losses at 1068 nm, as a function of the waveguides width, obtained using the top-view technique [52], for the waveguides prepared without gold nanoparticles and using 10 and 20 min for the gold deposition are presented in Fig. 13(a). Fig. 13(b) shows the results of the relative gain at 805 nm (for the waveguides without gold nanoparticles and after 10 and 20 min of gold deposition) for a waveguide width of 30 μm. We note that the relative gain reaches 22 dB/cm for the waveguide prepared with 10 min of gold deposition The increase of the

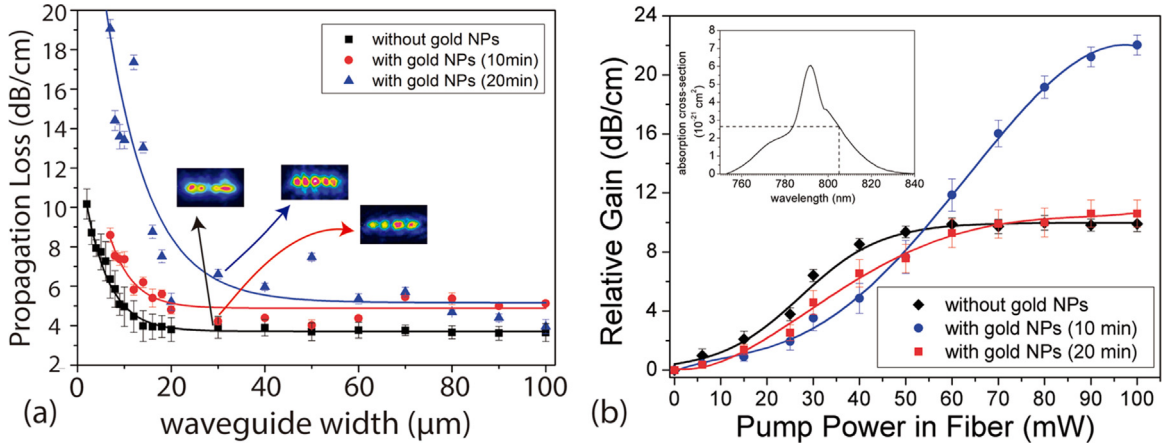

Fig. 13. (a) Propagation losses of Tm^{3+}/Yb^{3+} codoped PbO-GeO_2 pedestal waveguides (without gold NPs, and after 10 and 20 min of gold NPs deposition) as a function of the waveguides width. Inset shows the near-field profile for 30 μm waveguide width. (b) Relative gain as a function of pump power for 30 μm waveguide width (without gold NPs and with gold NPs for 10 and 20 min of gold deposition). The pump and signal wavelengths were 980 and 800 nm, respectively; the inset shows the absorption cross section profile of the Tm^{3+} $^3H_6 \rightarrow {}^3H_4$ transition (absorption cross section at 805 nm is $\approx 2.63 \times 10^{-21}$ cm^2) [36].

propagation losses and the relative gain decrease for 20 min of gold deposition were attributed to the reduced electric field enhancement and higher ohmic losses due to the nucleation of bigger gold nanoparticles [62,63]. This was the first report related to the use of pedestal structures with a thin cover layer of gold over the core, that showed the possibility to fabricate waveguides with applications on fiber network at short distances to operate at the first telecom window.

Rib waveguides based on Yb^{3+}/Er^{3+} codoped PbO-GeO_2 materials [64], with the same composition of the samples studied in the work mentioned above, achieved a maximum gain of 2 dB/cm, at 1.53 μm, which is three times smaller than the one obtained for the GP-B waveguide. It was only with the deposition of gold nanoparticles over the waveguides core, following the procedure mentioned previously, that the gain was increased and reached 4.3 dB/cm [64]. The gain enhancement was correlated to the luminescence enhancement of about 30% (Fig. 14) being attributed to the local field growth in the vicinity of the nanoparticles. Therefore, it was possible to conclude that the pedestal architecture can be used for optical amplifiers applications with advantages over rib waveguides. Also it is important to add that it was reported the use of the rib architecture for Ge and ZnSe thin films [65,66] and, in both cases, the etching technique was used after the electron beam or photolithography processes, respectively. During pedestal waveguides fabrication, the RIE occurs before the core definition and represents an alternative procedure for achieving the lateral

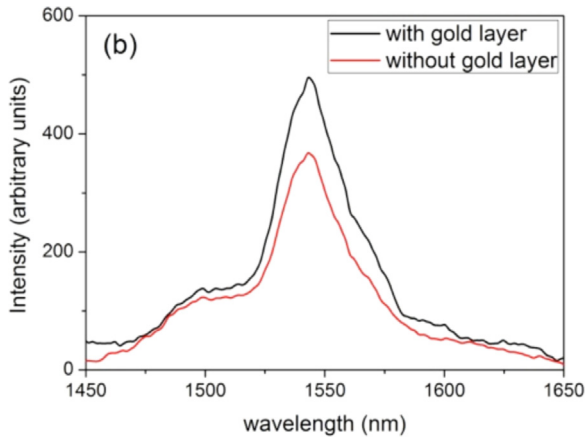

Fig. 14. The luminescence of Er^{3+}/Yb^{3+} doped PbO-GeO_2 thin films, with and without gold nanoparticles, in the near infrared region, under 980 nm excitation.

confinement in optical waveguides produced using the silicon technology. Besides, it is also an advantage when compared to the method used for rib waveguides fabrication since the material used as core layer does not need to be submitted to etching procedures, simplifying the fabrication process. We recall that the interest in pedestal-type waveguides has emerged recently because of the favorable characteristics for optical field confinement [47,53], even though the type of pedestal waveguide proposed in [47] is very different from the one we have proposed [1,34–36,49] as the sidewalls are really etched in ref [47].

Table 1 shows a comparative summary between some pedestal and rib type waveguides made from different materials. In the table is possible to verify in a straightforward way the advantage of using pedestal waveguides for optical amplification.

It was reported a procedure that reduced the propagation losses of integrated photonics waveguides based on the etchless process [67]. In this fabrication process, a mask of lower index material is defined over the waveguide core with sidewalls obtained by thermal oxidation. The mask composed of a dielectric, is not removed since it has a lower index when compared with the one of the core, and is usually of silicon. The oxidized layers on the sides and the masking material on top surround the silicon core. Thus the guiding mechanism is totally based on the internal reflection. In this way, although the waveguide sidewalls end up not are not perfectly vertical, which is not detrimental to the guiding performance, smaller losses were achieved. Losses as low as 0.3 dB/cm were obtained at 1.53 μm wavelength [67]. Ring resonators with quality factors as high as many hundreds of thousands were demonstrated using a similar process [68,69]. Unfortunately, the etchless process can only be used for materials that can be thermally oxidized and so has limitation that does not exist on the pedestal waveguide fabrication process that can be used with advantages over the etchless one too.

There is still a long way to go with respect to the integration of pedestal waveguides with other devices such as active electronic and optoelectronics devices such as semiconductor amplifiers, lasers, LEDs and photo-detectors. One possible way to integrate pedestals with sources and detectors or other opto-electronic components fabricated underneath the pedestals would be to use of thin resonant layers with different refractive indices, such as the ones used between the core and the lower cladding in ARROW waveguides [44]. If this resonant layer, called the anti-resonant layer in ARROW waveguide, is designed to let the optical mode leak towards the substrate, the optical power could be coupled to a photo-detector or other opto-electronic device fabricated on the semiconductor substrate previously. By simply tuning the thickness of this film, which works as a resonant layer, it can be ensured

Table 1
Summary of pedestal and rib waveguides with different materials.

Waveguide	Material	Gain (dB/cm)	Losses (dB/cm)
Pedestal	Yb^{3+}/Er^{3+} codoped $TeO_2-WO_3-Bi_2O_3$[35]	3.7	2.5 (1050 nm)
Rib	Er^{3+} codoped TeO_2 [53]	3.0	~ 0.4 (1100–1500 nm)
Pedestal	Er^{3+}/Yb^{3+} codoped $PbO-GeO_2$ (GP-B) [1]	6.0	1.0 (1068 nm)
Rib	Er^{3+}/Yb^{3+} codoped $PbO-GeO_2$ with gold nanoparticles [64]	4.3	1.0 (1050 nm)
Pedestal	Tm^{3+}/Yb^{3+} codoped PbO-GeO_2 with gold nanoparticles (10 min) [36]	22.0	5.0 (1068 nm)

that the condition for leakage to occur is satisfied. Regarding LASERs it is theoretically possible to fabricate structures like Distributed Feedback (DFB) LASERs and Distributed Bragg Reflectors (DBR) LASERs directly on the pedestals if semiconductors gain media are used as the core layer and corrugations are etched on this core. This would be feasible even though certainly many challenges would have to be overcome for it to be achieved.

4. Future perspectives of pedestal platform for integrated nonlinear optical devices applications

In this section, we discuss the significant potential of the pedestal platform for nonlinear optical devices applications. Pedestal waveguides fabricated with different core materials hold a great promise for these kinds of devices. As mentioned, choosing materials in such a way that a larger refractive index contrast between core and cladding takes place, makes integrated devices attractive due to the possibility of smaller mode dimensions, which lead to larger nonlinear parameters and shorter devices. Nonlinear devices such as Optical Parametric Amplifiers (OPAs) have been theoretically proven to have gain bandwidth larger than any other type of amplifier (over tens of terahertz). The actual implementation of these devices on optical networks has been hindered by Stimulated Brillouin Scattering (SBS), which needs to be suppressed for proper amplification [70–72]. Due to the very long fiber lengths required for OPAs, SBS is a compromising issue in fiber optics technology. Integrated photonics has the potential to be the perfect solution to make OPAs feasible, since devices with length on the centimeter scale can present the same overall gain as meters of kilometers of optical fiber [73–76].

A whole breadth of materials in the form of thin solid films hold great promise for being explored due to their high optical nonlinear susceptibilities. As an example, we can cite all the materials that have been proposed as high-k dielectrics for MOS transistors and capacitors. Some of these materials, like nanocrystalline titanium dioxide (TiO_2), hafnium dioxide (HfO_2) and zirconium dioxide (ZrO_2) have high third order nonlinear susceptibilities [77–81]. In spite of this, developing etch recipes that lead to smooth sidewalls and hence low propagation loss waveguides are a challenge due to the fact that they are based on transition metals. Here as well, the pedestal process has potential to be hugely beneficial.

Besides allowing the exploration of novel materials, pedestal waveguides would allow more degrees of freedom for dispersion engineering of the waveguide. It is well known that the nonlinear processes such as Four Wave Mixing (FWM) which is the basis of the parametric amplification, wavelength conversion and frequency comb generation, among others, requires the waveguide or material medium to have certain tuned dispersion characteristics at the central pump wavelength [82]. In optical fibers and integrated waveguides, the material dispersion as well as the geometric dimensions are tuned in order to have an appropriate dispersion. This is known as dispersion engineering and it consists on simply optimizing the width and height of a strip waveguide, for example, in order to have an appropriate dispersion, which leads to gain in nonlinear processes [83]. As it can be seen in Fig. 15, pedestal waveguides have more geometric features, and hence, more degrees of freedom that can be tuned in order to realize dispersion engineering. As opposed to strip waveguides, where only

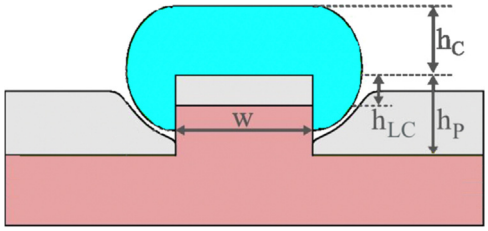

Fig. 15. Illustration of the geometric parameters that can be varied in order to do the dispersion engineering to phase match nonlinear processes.

strip height and width can be tuned, in pedestal waveguides, the pedestal width W, height h_P, core height h_C and lower cladding height h_{LC} can be varied until the desired dispersion is achieved. This can be explained by the fact that the pedestal can be etched beyond the lower cladding thickness. In this way, waveguides that lead to larger amplifier gain or gain with flatter spectrum response can be designed.

Novel materials like PbO-GeO_2 have great potential for nonlinear optics applications if proper dispersion engineering is used. It was reported in ref [60] a large nonlinear absorption coefficient at 532 nm, indicating the possible use of PbO-GeO_2 thin films with gold nanoparticles for optical limiting in the picosecond regime. In the same work it was shown the nonlinear refractive index enhancement at 532 (15 ps) and 800 nm (100 fs) due to the presence of gold nanoparticles by more than two orders of magnitude. Nonlinear refractive index of 10^{-12} cm^2/W was found, at 800 nm, and demonstrated that PbO-GeO_2 materials are good candidates for optical switching [61]. Third-order optical nonlinearities in PbO-GeO_2 glasses with silver nanoparticles were investigated at visible and infrared wavelengths [84]. The results demonstrated that they are good candidates for the development of all-optical switching at 700–1400 nm (120 fs); the experiments performed at the visible range showed that they behave either as a saturable absorber (below 450 nm) or as an optical limiter (480–550 nm). These glasses present nonlinear refractive index of 12.10^{-16} cm^2/W, at 1300 nm, three times larger than those reported for lead oxifluoroborate glasses [85] but similar to the one reported for glass-ceramic containing sodium niobate nanocrystals [86] Since this material was used to fabricate the pedestal waveguides presented in this work, they can be a good alternative for the production of different nonlinear devices as well. Other materials could be explored as well for integrated nonlinear optical devices fabrication, and the pedestal platform would be ideal to test these materials since it does not require the etching of the core and is better suited for dispersion engineering as discussed above.

We emphasize that the use of pedestal waveguides for nonlinear optics applications requires accurate design of the geometrics dimensions, in order to achieve adequate dispersion that allows gain in Four Wave Mixing (FWM) or any other nonlinear process that is the base for several nonlinear optical devices such as Frequency Comb Generators, Optical Parametric Amplifiers among others.

5. Conclusions

We have reviewed recent reports of pedestal waveguide technology that can be used to explore novel materials opening new possibilities in

the field of photonics. As the material used as core layer does not need to be submitted to etching procedures, the fabrication process is simplified. So, this technology raises the possibility to explore novel materials including those that are inert to chemical etchants. The reduction of the losses due to micro-masking and roughness pattern transfer from the hard-mask also represent another advantage that can contribute to the development of new photonic devices in the future. Results of Mach Zehnder structures were demonstrated using TeO_2–WO_3–Bi_2O_3 pedestal waveguides with different widths and showed that low loss (2.0 dB cm^{-1} and 2.5 dB cm^{-1} at 633 and 1050 nm, respectively) waveguides could be constructed with tellurite-based materials for integrated optical sensors applications. Yb^{3+}/Er^{3+} codoped TeO_2–WO_3–Bi_2O_3 pedestal waveguides were reviewed for optical amplifier applications at 1530 nm. Gain of 3.7 dB cm^{-1} was achieved at 1530 nm, under 980 nm excitation, for waveguides width of 20 μm. Advances on the pedestal waveguides fabrication process allowed the construction of amplifiers with better performance. In this case it was possible to observe for Yb^{3+}/Er^{3+} PbO-GeO_2 waveguides reduction of about 50% for the propagation losses at 632 and 1068 nm, and enhancement of about 50%, for 70 μm width waveguides, at 1530 nm. These results motivated the construction of Yb^{3+}/Tm^{3+} doped GeO_2-PbO pedestal waveguides for operation at the first telecommunication window at 805 nm and led to interesting results that are were reviewed in the present work So, in this case, relative gain enhancement of more than 100% was observed at 805 nm due to the presence of gold nanoparticles for a waveguide width of 30 μm that reached 22 dB/cm favoring applications with fiber network at short distances to operate at the first telecom window. We have also shown that novel materials for other applications, such as integrated nonlinear optics, have enormous potential due to the reasons mentioned above and also to the possibility of better dispersion engineering.

Acknowledgment

We acknowledge the financial support from the National Institute of Photonics (INCT de Fotônica) supported by the Conselho Nacional de Desenvolvimento Científico e Tecnológico (CNPq) (465763/2014-6). The authors would also like to acknowledge Emerson G. Melo for the relevant contributions during the discussion of the results.

References

[1] F.A. Bomfim, D.M. da Silva, L.R.P. Kassab, T.A.A. de Assumpção, V.D. Del Cacho, M.I. Alayo, Advances on the fabrication process of Er^{3+}/Yb^{3+}:GeO_2–PbO pedestal waveguides for integrated photonics, Opt. Mater. 49 (2015) 196–200.
[2] T.F. Xu, X. Shen, Q.H. Nie, Y. Gao, Spectral properties and thermal stability of Er^{3+}/Yb^{3+} codoped tungsten–tellurite glasses, Opt. Mater. 28 (2006) 241–245.
[3] H. Lin, S. Tanabe, L. Lin, Y.Y. Hou, K. Lin, D.L. Yang, T.C. Ma, J.Y. Yu, E.Y.B. Pun, Near-infrared emissions with widely different widths in two kinds of Er^{3+}-doped oxide glasses with high refractive indices and low phonon energies, J. Lumin. 124 (2007) 167–172.
[4] L. Bontempo, S.G. dos Santos Filho, L.R.P. Kassab, Conduction and reversible memory phenomena in Au-nanoparticles-incorporated TeO_2–ZnO films, Thin Solid Films 611 (2016) 21–26.
[5] Y. Wu, X. Shen, S. Dai, Y. Xu, F. Chen, C. Lin, T.F. Xu, Q.H. Nie, Silver nanoparticles enhanced upconversion luminescence in Er^{3+}/Yb^{3+} codoped bismuth-germanate glasses, J. Phys. Chem. 115 (2011) 25040–25045.
[6] M.E. Camilo, E.O. Silva, L.R.P. Kassab, J.A.M. Garcia, C.B. de Araújo, White light generation controlled by changing the concentration of silver nanoparticles hosted by $Ho^{3+}/Tm^{3+}/Yb^{3+}$ doped GeO_2–PbO glasses, J. Alloy. Compd. 644 (2015) 155–158.
[7] L.A. Florêncio, L.A. Gomez-Malagón, B.C. Lima, A.S.L. Gomes, J.A.M. Garcia, L.R.P. Kassab, Efficiency enhancement in solar cells using photon down-conversion in Tb/Yb-doped tellurite glass, Sol. Energy Mater. Sol. Cells 157 (2016) 468–475.
[8] W.H. Dumbaugh, Lead bismuthate glasses, Phys. Chem. Glass. 19 (1978) 121–125.
[9] W.H. Dumbaugh, Heavy metal oxide glasses containing Bi_2O_3, Phys. Chem. Glass. 27 (1986) 119–123.
[10] W.A. Pisarski, J. Pisarska, G. Dominiak-Dzik, M. Maczkac, W. Ryba-Romanowski, Compositional-dependent lead borate based glasses doped with Eu^{3+} ions: synthesis and spectroscopic properties, J. Phys. Chem. Solids 67 (2006) 2452–2457.
[11] H. Lin, G. Meredith, S. Jiang, X. Peng, T. Luo, N. Peyghambarian, E.Y.-B. Pun, Optical transitions and visible upconversion in Er^{3+} doped niobic tellurite glass, J. Appl. Phys. 93 (2003) 186–191.
[12] D. Rajesh, M.R. Dousti, R.J. Amjad, A.S.S. de Camargo, Enhancement of down- and upconversion intensities in Er^{3+}/Yb^{3+} co-doped oxyfluoro tellurite glasses induced by Ag species and nanoparticles, J. Lumin. 192 (2017) 250–255.
[13] X. Shen, Q.H. Nie, T.F. Xu, Y. Gao, Optical transitions of Er^{3+}/Yb^{3+} codoped TeO_2–WO_3–Bi_2O_3 glass, Spectrochim. Acta Part A 61 (2005) 2827–2831.
[14] T. Som, B. Karmakar, Enhancement of Er^{3+} upconverted luminescence in Er^{3+}: au-antimony glass dichroic nanocomposites containing hexagonal Au nanoparticles, J. Opt. Soc. Am. B 26 (2009) B21–B27.
[15] B. Klimesz, G. Dominiak-Dzik, P. Solarz, M. Zelechower, W. Ryba-Romanowski, Optical study of GeO2–PbO–PbF2 oxyfluoride glass singly doped with Pr^{3+}, Nd^{3+}, Sm^{3+} and Eu^{3+}, J. Alloy. Compd. 403 (2005) 76–85.
[16] A. Ghosh, R. Debnath, Judd–Ofelt analysis of Er^{+3} activated lead free fluoro–tellurite glass, Opt. Mater. 31 (2009) 604–608.
[17] G. Lakshminarayana, H. Yang, J.R. Qiu, White light emission from Tm^{3+}/Dy^{3+} co-doped oxyfluoride germanate glasses under UV light excitation, J. Solid State Chem. 182 (2009) 669–676.
[18] G. Lakshminarayana, R. Yang, J.R. Qiu, M.G. Brik, G.A. Kumar, I.V. Kityk, White light emission from Sm^{3+}/Tb^{3+} codoped oxyfluoride aluminosilicate glasses under UV light excitation, J. Phys. D: Appl. Phys. 42 (2009) 015414.
[19] C.B. de Araújo, L.R.P. Kassab, Chapter 5 - Enhanced photoluminescence and planar waveguides of rare-earth doped germanium oxide glasses with metallic nanoparticles, in: B. Karmakar, K. Rademann, A.L. Stepanov Glass (Eds.), Nanocomposites: Preparation, Properties, and Applications, William Andrew Publishing, Boston, 2016, pp. 131–144.
[20] M.R. Dousti, M.R. Sahar, R.J. Amjad, S.K. Ghoshal, A. Awang, Surface enhanced Raman scattering and up-conversion emission by silver nanoparticles in erbium–-zinc–tellurite glass, J. Lumin. 143 (2013) 368–373.
[21] M.R. Dousti, M.R. Sahar, M.S. Rohani, A. Samavati, Z.A. Mahraz, R.J. Amjad, A. Awang, R. Arifin, Nano-silver enhanced luminescence of Eu_{3+}-doped lead tellurite glass, J. Lumin. 1065–1066 (2014) 39–42.
[22] L.M. Moreira, V. Anjos, M.J.V. Bell, C.A.R. Ramos, L.R.P. Kassab, D.J.L. Doualan, P. Camy, R. Moncorgé, The effects of Nd_2O_3 concentration in the laser emission of TeO_2-ZnO glasses, Opt. Mater. 58 (2016) 84–88.
[23] S.P. Zimin, E.S. Gorlachev, I.I. Amirov, H. Zogg, Micromasking effect and nanostructure self-formation on the surface of lead chalcogenide epitaxial films on Si substrates during argon plasma treatment, J. Phys. D: Appl. Phys. 42 (2009) 165205.
[24] D.O. Carvalho, M.I. Alayo, Pedestal Anti-resonant Reflecting Optical Waveguides, in: Proceedings of the SPIE 7940, Oxide-based Materials and Devices II, pp. 794017-1–794017-8, 2011.
[25] D. Yin, H. Schmidt, J.P. Barber, A.R. Hawkins, Integrated ARROW waveguides with hollow cores, Opt. Express 12 (2004) 2710–2715.
[26] A.G. Griffith, R.K.W. Lau, J. Cardenas, Y. Okawachi, A. Mohanty, R. Fain, Y.H.D. Lee, M. Yu, C.T. Phare, C.B. Poitras, A.L. Gaeta, M. Lipson, Silicon-chip mid-infrared frequency comb generation, Nat. Commun. 6 (2015) 6299.
[27] L. Xu, N. Ophir, M. Menard, R.K.W. Lau, A.C. Turner-Foster, M.A. Foster, M. Lipson, A.L. Gaeta, K. Bergman, Simultaneous wavelength conversion of ASK and DPSK signals based on four-wave-mixing in dispersion engineered silicon waveguides, Opt. Express 19 (2011) 12172–12179.
[28] N. Ophir, J. Chan, K. Padmaraju, A. Biberman, A.C. Foster, M.A. Foster, M. Lipson, A.L. Gaeta, K. Bergman, Continuous Wavelength Conversion of 40-Gb/s Data Over 100 nm Using a Dispersion-Engineered Silicon Waveguide, IEEE Photonics Technol. Lett. 23 (2011) 73–75.
[29] J.S. Levy, K. Saha, Y. Okawachi, M.A. Foster, A.L. Gaeta, M. Lipson, High-performance silicon-nitride-based multiple-wavelength source, IEEE Photonics Technol. Lett. 24 (2012) 1375–1377.
[30] A. Pasquazi, Y. Park, J. Azaña, F. Légaré, R. Morandotti, B.E. Little, S.T. Chu, D.J. Moss, Efficient wavelength conversion and net parametric gain via Four Wave Mixing in a high index doped silica waveguide, Opt. Express 18 (2010) 7634–7641.
[31] Y. Okawachi, M. Yu, K. Luke, D.O. Carvalho, S. Ramelow, A. Farsi, M. Lipson, A.L. Gaeta, Dual-pumped degenerate Kerr oscillator in a silicon nitride microresonator, Opt. Lett. 40 (2015) 5267–5270.
[32] K.J.A. Ooi, D.K.T. Ng, T. Wang, A.K.L. Chee, S.K. Ng, Q. Wang, L.K. Ang, A.M. Agarwal, L.C. Kimerling, D.T.H. Tan, Pushing the limits of CMOS optical parametric amplifiers with USRN:Si_7N_3 above the two-photon absorption edge, Nat. Commun. 8 (2017) 13878.
[33] L. Razzari, D. Duchesne, M. Ferrera, R. Morandotti, S. Chu, B.E. Little, D.J. Moss, CMOS-compatible integrated optical hyper-parametric oscillator, Nat. Photonics 4 (2010) 41–45.
[34] M.E. Camilo, L.R.P. Kassab, T.A.A. Assumpção, V.D.D. Cacho, M.I. Alayo, Fabrication and characterization of pedestal optical waveguides using TeO_2–WO_3–Bi_2O_3 thin film as core layer, Thin Solid Films 571 (2014) 225–229.
[35] V.D. Del Cacho, D.M. da Silva, T.A.A. de Assumpção, L.R.P. Kassab, M.I. Alayo, E.G. Melo, Fabrication of Yb^{3+}/Er^{3+} codoped Bi_2O_3–WO_3–TeO_2 pedestal type waveguide for optical amplifiers, Opt. Mater. 38 (2014) 198–203.
[36] T.A.A. de Assumpção, M.E. Camilo, M.I. Alayo, D.M. da Silva, L.R.P. Kassab, Influence of gold nanoparticles on the 805 nm gain in Tm^{3+}/Yb^{3+} codoped PbO-GeO_2 pedestal waveguides, Opt. Mater. 72 (2017) 518–523.
[37] T. Begou, B. Bêche, N. Grossard, J. Zyss, A. Goullet, G. Jézéquel, E. Gaviot, Marcatili's extended approach: comparison to semi-vectorial methods applied to pedestal waveguide design, J. Opt. A: Pure Appl. Opt. 10 (2008) 055310.
[38] E.A.J. Marcatili, Dielectric rectangular waveguide and directional coupler for integrated optics, Bell Syst. Tech. J. 48 (1969) 2071–2102.
[39] B. Bêche, J.F. Jouin, N. Grossard, E. Gaviot, E. Toussaere, J. Zyss, PC software for analysis of versatile integrated optical waveguides by polarised semi-vectorial finite difference method, Sens. Actuators A 114 (2004) 59–64.

[40] D. Marcuse, Solution of the vector wave equation for general dielectric waveguides by the Galerkin method, IEEE J. Quantum Electron. 28 (1992) 459–465.
[41] N. Grossard, Etude théorique et exp´érimentale d'um convertisseur de polarisation intégré sur semiconducteurs de type III-V, Thesis of University of Franche-Comté Besanc on-France.
[42] R.L. Gallawa, I.C. Goyal, Y. Tu, K. Ghatak, Optical waveguide modes: an approximate solution using Galerkin's method with Hermite-Gauss basis functions, IEEE J. Quantum Electron. 27 (1991) 518–522.
[43] Y. Chen, J. Feng, Z. Zhou, J. Yu, C.J. Summers, D.S. Citrin, Fabrication of silicon microring resonator with smooth sidewalls, J. Micro/Nanolithogr., MEMS, MOEMS 8 (2009) 043060.
[44] E.G. Melo, M.I. Alayo, D.O. Carvalho, Study of the pedestal process for reducing sidewall scattering in photonic waveguides, Opt. Express 25 (2017) 9755–9760.
[45] M.A. Alvarado, M.V. Pelegrini, I. Pereyra, T.A.A. de Assumpção, L.R.P. Kassab, M.I. Alayo, Fabrication and characterization of aluminum nitride pedestal-type optical waveguide, Can. J. Phys. 92 (2014) 951–954.
[46] D.O. Carvalho, M.I. Alayo, a-SiC:H anti-resonant layer ARROW waveguides, J. Opt. A: Pure Appl. Opt. 10 (2008) 104002.
[47] J. Cheng, W. Zhang, Q. Zhou, Y. Wang, Y. Huang, J. Peng, Single polarization transmission in pedestal-supported silicon waveguides, Opt. Lett. 36 (2011) 1797–1799.
[48] L.G. de Peralta, A.A. Bernussi, H. Temkin, M.M. Borhani, D.E. Doucette, Silicon-dioxide waveguides with low birefringence, IEEE J. Quantum Electron. 39 (2003) 874–879.
[49] T.A.A. de Assumpção, M.A. Alvarado, M.I. Alayo, L.R.P. Kassab, Production and characterization of Tm^{3+}/Yb^{3+} codoped pedestal-type PbO–GeO_2 waveguides, Can, J. Phys. 92 (2014) 597–601.
[50] T.A.A. de Assumpção, D.M. da Silva, V.D. Del Cacho, L.R.P. Kassab, M.I. Alayo, Production and characterization of Tm3+/Yb3+ codoped waveguides based on PbO–GeO2 thin films, J. Alloy. Compd. 586 (2014) S368–S372.
[51] K. Okamoto, Fundamentals of Optical Waveguides, second ed., Academic Press, Burlington, 2006.
[52] Y. Okamura, S. Yoshinaka, S. Yamamoto, Measuring mode propagation losses of integrated optical waveguides: a simple method, Appl. Opt. 22 (1983) 3892–3894.
[53] K. Vu, S. Farahani, S. Madden, 980nm pumped erbium doped tellurium oxide planar rib waveguide laser and amplifier with gain in S, C and L band, Opt. Express 23 (2015) 747–755.
[54] M.A. Webster, R.M. Pafchek, A. Mitchell, T.L. Koch, Width Dependence of Inherent TM-Mode Lateral Leakage Loss in Silicon-On-Insulator Ridge Waveguides, IEEE Photonics Technol. Lett. 19 (2007) 429–431.
[55] S.P.A. Osorio, V.A.G. Rivera, L.A.O. Nunes, E. Marega Jr., D. Manzani, Y. Messaddeq, Plasmonic Coupling in Er^{3+}:Au Tellurite Glass, Plasmonics 7 (2012) 53–58.
[56] L.R.P. Kassab, D.S. da Silva, R. de Almeida, C.B. Araújo, Photoluminescence enhancement by gold nanoparticles in Eu^{3+} doped GeO_2–Bi_2O_3 glasses, Appl. Phys. Lett. 94 (2009) 101912.
[57] V.A.G. Rivera, Y. Ledemi, S.P.A. Osorio, D. Manzani, Y. Messaddeq, L.A.O. Nunes, E. Marega Jr., Efficient plasmonic coupling between Er^{3+}:(Ag/Au) in tellurite glasses, J. Non-Cryst. Solids 358 (2012) 399–405.
[58] D.S. da Silva, T.A.A. de Assumpção, L.R.P. Kassab, C.B. de Araújo, Frequency up-conversion in Nd^{3+} doped PbO–GeO_2 glasses containing silver nanoparticles, J. Alloy. Compd. 586 (2014) S516–S519.
[59] L.A. Gómez, F.E.P. dos Santos, A.S.L. Gomes, C.B. de Araújo, L.R.P. Kassab, W.G. Hora, Near-infrared third-order nonlinearity of PbO–GeO_2 films containing Cu and Cu_2O nanoparticles, Appl. Phys. Lett. 92 (2008) 141916.
[60] D.M. da Silva, L.R.P. Kassab, J.R. Martinelli, C.B. de Araújo, Production and characterization of RF-sputtered PbO-GeO_2 amorphous thin films containing silver and gold nanoparticles, J. Non-Cryst. Solids 356 (2010) 2602–2605.
[61] C.B. de Araújo, T.R. Oliveira, E.L. Falcão-Filho, D.M. Silva, L.R.P. Kassab, Nonlinear optical properties of PbO–GeO_2 films containing gold nanoparticles, J. Lumin. 133 (2013) 180–183.
[62] Nagaraj, A.A. Krokhin, Long-range surface plasmons in dielectric-metal-dielectric structure with highly anisotropic substrates, Phys. Rev. B 81 (2010) 085426.
[63] P. Berini, Long-range surface plasmon polaritons, Adv. Opt. Photonics 1 (2009) 484–588.
[64] D.M. da Silva, L.R.P. Kassab, A.L. Siarkowski, C.B. de Araújo, Influence of gold nanoparticles on the 1.53 μm optical gain in Er^{3+}/Yb^{3+}: PbO-GeO_2 RIB waveguides, Opt. Express 22 (2014) 16424–16430.
[65] J. Kang, M. Takenaka, S. Takagi, Novel Ge waveguide platform on Ge-on-insulator wafer for mid-infrared photonic integrated circuits, Opt. Express 24 (2016) 11855–11864.
[66] V. Mittal, N.P. Sessions, J.S. Wilkinson, G.S. Murugan, Optical quality ZnSe films and low loss waveguides on Si substrates for mid-infrared applications, Opt. Mater. Express 7 (2017) 712–725.
[67] J. Cardenas, C.B. Poitras, J.T. Robinson, K. Preston, L. Chen, M. Lipson, Low loss etchless silicon photonic waveguides, Opt. Express 17 (2009) 4752–4757.
[68] L.W. Luo, G.S. Wiederhecker, J. Cardenas, C. Poitras, M. Lipson, High quality factor etchless silicon photonic ring resonators, Opt. Express 19 (2011) 6284–6289.
[69] A. Griffith, J. Cardenas, C.B. Poitras, M. Lipson, High quality factor and high confinement silicon resonators using etchless process, Opt. Express 20 (2012) 21341–21345.
[70] D. Cotter, Stimulated Brillouin scattering in monomode optical fiber, J. Opt. Commun. 4 (1983) 10–19.
[71] A. Kobyakov, M. Sauer, D. Chowdhury, Stimulated Brillouin scattering in optical fibers, Adv. Opt. Photonics 2 (2010) 1–59.
[72] F.H. Tithi, M.S. Islam, M.T.A. Tanna, Overview of stimulated Brillouin scattering effect and various types of method to eliminate this effect, Int. J. Comput. Appl. 92 (2014) 23–26.
[73] M.A. Khalil, G. Vitrant, Optical parametric amplification in composite polymer/ion exchanged planar waveguide, Appl. Phys. Lett. 77 (2000) 3713.
[74] X. Liu, R.M. Osgood Jr, Y.A. Vlasov, W.M.J. Green, Mid-infrared optical parametric amplifier using silicon nanophotonic waveguides, Nat. Photonics 4 (2010) 557–560.
[75] J.D. Marconi, M.L.F. Abbade, C.M. Serpa-Imbett, E.A.M. Fagotto, Ultra-broadband two-pump optical parametric amplifier in tellurite waveguides with engineered dispersion, Opt. Express 25 (2017) 4268–4283.
[76] S. Kumar, M. Sen, High-gain, low-threshold and small-footprint optical parametric amplifier for photonic integrated circuits, J. Opt. Soc. Am. B 35 (2018) 362–371.
[77] K. Iliopoulos, G. Kalogerakis, D. Vernardou, N. Katsarakis, E. Koudoumas, S. Couris, Nonlinear optical response of titanium oxide nanostructured thin films, Thin Solid Films 518 (2009) 1174–1176.
[78] V. Gayvoronsky, A. Galas, E. Shepelyavyy, Th Dittrich, V. Yu. Timoshenko, S.A. Nepijko, M.S. Brodyn, F. Koch, Appl. Phys. B: Lasers Opt. 80 (2005) 97–100.
[79] S.W. Yu, H.B. Liao, W.J. Wen, G.K.L. Wong, Au/TiO_2/SiO_2 sandwich multilayer composite films with large nonlinear optical susceptibility, Opt. Mater. 27 (2005) 1433–1437.
[80] S.S. Lin, H.R. Li, The optical properties of hydrophilic Hf-doped HfO_2 nanoceramic films, Ceram. Int. 39 (2013) 7677–7683.
[81] R.A. Ganeev, M. Morita, A.I. Ryasnyanskii, M. Baba, D. Rau, H. Fujii, M. Suzuki, M. Turu, H. Kuroda, Nonlinear optical characteristics of CdS and ZnS nanoparticles implanted into zirconium oxide thin films, Opt. Spectrosc. 97 (2004) 580–587.
[82] G.P. Agrawal, Nonlinear Fiber Optics, in: P.L. Christiansen, M.P. Sorensen, A.C. Scott (Eds.), Nonlinear Science at the Dawn of the 21st Century. Lecture Notes in Physics, Springer, Berlin, Heidelberg, 2000, pp. 195–211.
[83] Y. Okawachi, M.R.E. Lamont, K. Luke, D.O. Carvalho, M. Yu, M. Lipson, A.L. Gaeta, Bandwidth shaping of microresonator-based frequency combs via dispersion engineering, Opt. Lett. 39 (2014) 3535–3538.
[84] L. De Boni, E.C. Barbano, T.A. de Assumpção, L. Misoguti, L.R.P. Kassab, S.C. Zilio, Femtosecond third-order nonlinear spectra of lead-germanium oxide glasses containing silver nanoparticles, Opt. Express 20 (2012) 6844–6850.
[85] J.M.P. Almeida, L. De Boni, A.C. Hernandes, C.R. Mendonça, Third-order nonlinear spectra and optical limiting of lead oxifluoroborate glasses, Opt. Express 19 (2011) 17220–17225.
[86] E.L. Falcão-Filho, C.A.C. Bosco, G.S. Maciel, L.H. Acioli, C.B. de Araújo, A.A. Lipovskii, D.K. Tagantsev, Third-order optical nonlinearity of a transparent glass ceramic containing sodium niobate nanocrystals, Phys. Rev. B 69 (2004) 134204.